

# Robust method for broadband efficiency enhancement of electron photocathodes using optical interferences

Cite as: AIP Advances 11, 065325 (2021); doi: 10.1063/5.0050691

Submitted: 26 March 2021 • Accepted: 3 June 2021 •

Published Online: 21 June 2021



View Online



Export Citation



CrossMark

A. Alexander,<sup>1,a)</sup> M. Gaowei,<sup>2</sup> S. Mistry,<sup>3</sup> J. Walsh,<sup>2</sup> F. Liu,<sup>1</sup> K. Evans-Lutterodt,<sup>2</sup> E. Stavitski,<sup>2</sup> V. Pavlenko,<sup>1</sup> J. Smedley,<sup>1</sup> and N. Moody<sup>1</sup>

## AFFILIATIONS

<sup>1</sup>Los Alamos National Laboratory, Mailstop H851, Los Alamos, New Mexico 87545, USA

<sup>2</sup>Brookhaven National Laboratory, Building 535-B, Upton, New York 11973, USA

<sup>3</sup>Helmholtz-Zentrum Berlin, Albert-Einstein Strasse 15, Berlin 12489, Germany

<sup>a)</sup>Author to whom correspondence should be addressed: [aalexander@lanl.gov](mailto:aalexander@lanl.gov)

## ABSTRACT

We demonstrate the key features of an interference cathode using both simulations and experiments. We deposit Cs<sub>3</sub>Sb photocathodes on Ag to produce an interference enhanced photocathode with 2–5× quantum efficiency (QE) enhancement using a robust procedure that requires only a smooth metal substrate and QE monitoring during growth. We grow both an interference cathode (Ag substrate) and a typical photocathode (Si reference substrate) simultaneously to confirm that the effects are due to optical interactions with the substrate rather than photocathode composition or surface electron affinity differences. Growing the cathodes until the QE converges shows both the characteristic interference peaks during growth and the identical limiting case where the cathode is “infinitely thick,” in agreement with simulations. We also grow a cathode until the QE on Ag peaks and then stop the growth, demonstrating broadband QE enhancement.

© 2021 Author(s). All article content, except where otherwise noted, is licensed under a Creative Commons Attribution (CC BY) license (<http://creativecommons.org/licenses/by/4.0/>). <https://doi.org/10.1063/5.0050691>

Photocathode electron sources are used in a variety of applications, including ultrafast electron diffraction/microscopy (UED/UEM), low light detection sensors, XFELs, and induction accelerators.<sup>1–9</sup> UED and x-ray free electron laser (XFEL) applications require high brightness (low emittance and high efficiency) and a fast time response.<sup>5,10</sup> This poses challenges, as basic physics models link the quantum efficiency (QE) and energy spread (emittance) of photocathodes through the concept of excess energy (defined as  $E_{\text{photon}} - \text{the work function } \phi$ <sup>11</sup>). Increasing the excess energy increases efficiency by increasing the number of scattering events that an excited electron can undergo before successfully being emitted from the photocathode surface. However, excess energy also increases the average kinetic energy of the emitted electron, and the resulting increase in the mean transverse energy (MTE) of the electron dominates the thermal emittance of the electron beam from a smooth, uniform photocathode.<sup>12</sup> Thus, a typical prescription for improving one figure of merit (cathode efficiency) leads to degradation in another of equal importance (emittance).

Improving QE without increasing emittance is an active area of research, with most efforts focused on reducing the MTE, e.g., through ultrasoft or single crystal photocathode materials, using subbands in heterostructures to produce emission resonances, or by enhancing optical absorption using nanostructures and heterostructures.<sup>5,13–17</sup> Interference cathodes use a single thin film photocathode on an optimized substrate to increase optical absorption and thus QE without increasing emittance, with two main advantages of alkali antimonide cathodes over other heterostructures that also enhance optical absorption. In particular, rough surfaces and nanostructures are known to increase emittance, which is challenging for applications such as XFELs and UEM that essentially require low emittance cathodes to be nearly atomically flat.<sup>18</sup> More complex planar heterostructures, such as distributed Bragg reflectors (DBRs), require extremely precise optical constants and process control to produce many layered structures. Alkali antimonides and other commonly used photocathode materials have limited optical data and poor stoichiometry control compared to most semiconductor materials

and are sufficiently reactive that producing precise multilayered heterostructures remains a challenge.<sup>19</sup> As a result, optical optimization of these materials requires a method that is robust to variations in optical properties and uses a single layer of the photocathode material.

Interference photocathodes work by using destructive interferences at the surface of the photocathode to eliminate reflection losses while using a low transmission substrate.<sup>20</sup> This increases the absorption inside the material. The interference effect also changes the energy distribution inside the material, producing electrons closer to the surface.<sup>20</sup> This reduces scattering losses. The combination increases the QE without changes in the excess energy or scattering mechanisms, thus increasing the QE without increasing emittance.

As seen in Fig. 1, the total elimination of reflection losses requires both amplitude and phase matching. Amplitude matching is typically achieved by optimizing the thickness of the material, as the absorption constant largely determines amplitude decay for a thin film on an infinitely thick substrate.<sup>21</sup> Both the photocathode itself and the substrate contribute to the phase shift, and for a given photocathode, a perfectly reflective metal with optimized optical constants would result in complete absorption inside the cathode. Practically, these materials do not exist, and the partial transmissivity and unoptimized phase shift in the real metals used as substrates result in both different optimal photocathode thicknesses and absolute absorption for different metal substrates.<sup>20</sup> This analysis assumes that both the substrate and cathode are smooth enough for the light to interact in a wave-like manner. Essentially, this requires the surface roughness to be much smaller than the wavelength of light used, which is difficult to achieve. Substrate or cathode surface roughness can destroy the wavefront, making it impossible to produce interferences. A common estimate for the degree of roughness that can destroy interferences is the Fraunhofer limit of  $\lambda/30$ .<sup>22</sup> This roughness requirement is challenging but possible (and desired/required for low emittance cathodes in particular).<sup>18</sup> While sub-nm roughness is common for single crystal silicon and other semiconductors, producing very smooth metal substrates requires either using polished single crystal metal substrates or using a very finely tuned evaporation process to deposit the metal onto an atomically smooth semiconductor. These requirements are also

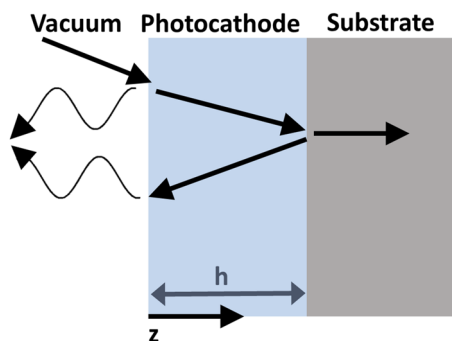
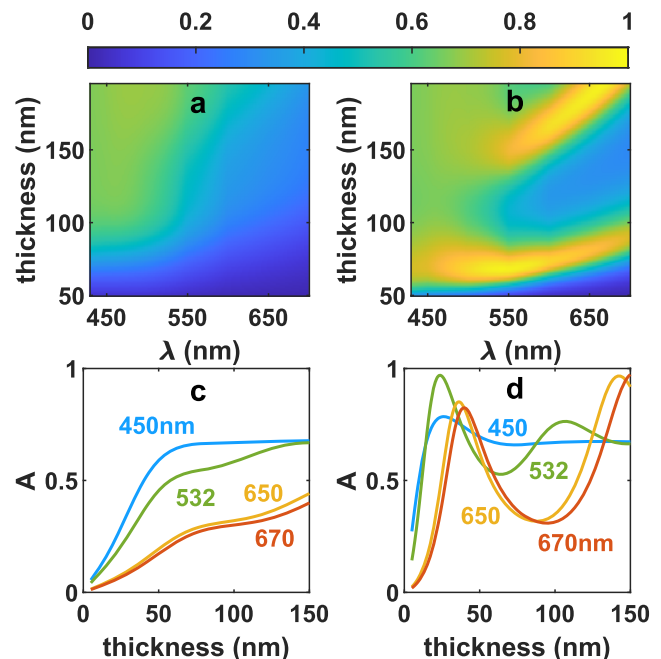


**FIG. 1.** Schematic of an interference cathode where destructive interferences at the surface and reduced transmission at the metal substrate result in enhanced absorption and QE in the photocathode.

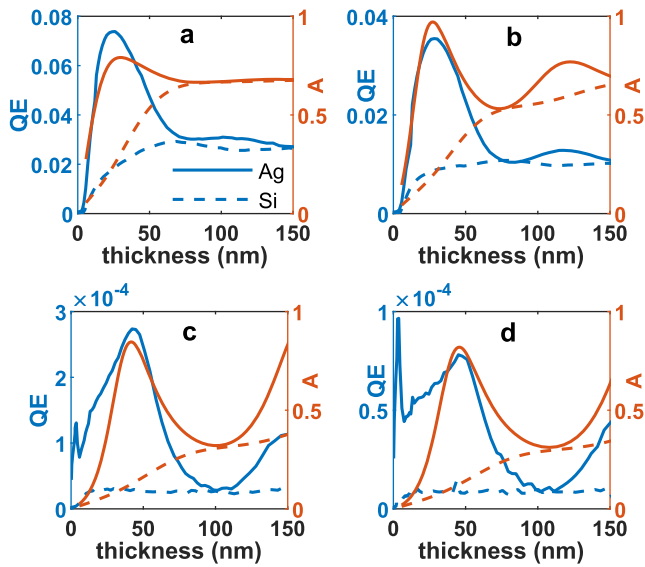
incompatible with sequential deposition techniques that are most commonly used to grow photocathodes but are achievable by using codeposition or sputtering, two techniques that have recently been developed.<sup>23,24</sup> This likely explains why interference cathodes previously posited in the literature were never rigorously experimentally confirmed or were modeled using incoherent light.<sup>25–27</sup>

Figure 2 shows the simulated spectral absorptance (derived in Ref. 20) of a Cs<sub>3</sub>Sb cathode<sup>28</sup> on an Ag<sup>29</sup> and Si<sup>30</sup> substrate, respectively. The equations used assume perfectly flat, parallel surfaces and normal incidence light with an infinitely thick substrate. The optical calculations give insights into the signatures that could confirm the experimental presence of an interference cathode. First, note that for a given wavelength, absorption for Cs<sub>3</sub>Sb on Ag peaks at a specific thickness due to the interference, in contrast to absorption on Si, where high transmission at the photocathode–substrate interface results in a monotonic increase in absorption. Second, note that as thickness increases, the size of these peaks or oscillations decreases, with an infinitely thick cathode having a constant absorption equal to  $1 - R$ , where R is the angle dependent Fresnel reflection coefficient between vacuum and the photocathode. The absorption peaks decay more quickly at shorter wavelengths due to both the shorter length scales and higher absorption coefficients. This also results in a shift in the peak absorption to larger thicknesses as the wavelength increases. Changing optical constants over the visible range result in broadband absorption enhancement, without the absorption oscillations over the wavelength spectrum that would be expected if the refractive index was constant.

These effects are demonstrated experimentally in Fig. 3, which shows the QE of the as-grown Cs<sub>3</sub>Sb cathode simultaneously



**FIG. 2.** Simulated spectral absorptance of a Cs<sub>3</sub>Sb cathode grown on Si (a) and Ag (b), with cutouts for key wavelengths (450, 532, 650, and 670 nm) on Si (c) and Ag (d).



**FIG. 3.** Absorption simulations (red) and experimental QE data (blue) of a Cs<sub>3</sub>Sb photocathode grown on Ag (solid line) and Si (dashed) illuminated by different light wavelengths: 450 nm (a), 532 nm (b), 650 nm (c), and 670 nm (d).

grown by codeposition on Ag and Si substrates at multiple wavelengths. Single crystal  $\langle 100 \rangle$  Ag substrates with roughness  $< 5$  nm were used.<sup>31</sup> Si substrates are also  $\langle 100 \rangle$  and were prepared as in Ref. 32 to remove native oxides. The film was grown using codeposition at a growth rate of 0.1 A/s and a substrate temperature of 80° C. Previous work demonstrated that both the Si substrate preparation and the codeposition process result in very smooth surfaces for alkali antimonides, with  $< 1$  nm roughness on the substrate and  $< 3$  nm roughness of the codeposited film.<sup>23,32,33</sup> The thickness was determined using a quartz-crystal microbalance (QCM) with a 15% geometry factor. The films were characterized using XRD after the growth as detailed in Ref. 32. The QE of the growing films is compared with the optical absorption simulations in Fig. 2. There are clear QE peaks at each wavelength on Ag near the optical absorption peaks predicted by our simulations. Furthermore, the QE of Cs<sub>3</sub>Sb on Ag has substantially higher peak QE than on the nearly infinitely thick Si substrate and shows substantial enhancement at almost all thicknesses  $< 50$  nm. This is evident at all four wavelengths measured during growth, showing broadband enhancement. Furthermore, the QE for Cs<sub>3</sub>Sb on Ag and Si converges at the end of the growth, indicating that the cathode is optically thick and that the cathodes are functionally identical. In addition, Fig. 3 demonstrates other features predicted by the model. As the wavelength increases, both simulations and data show that the peaks shift to larger thicknesses. A second smaller peak can be seen at higher thicknesses, with the second peak being more relatively prominent at larger wavelengths due to a reduced absorption constant. The second peak is dampened by both the optical absorption in the material and additional electron scattering losses resulting from the larger thickness.

Figure 4 demonstrates how an interference cathode can be grown, as well as its relative performance. The cathode was grown on

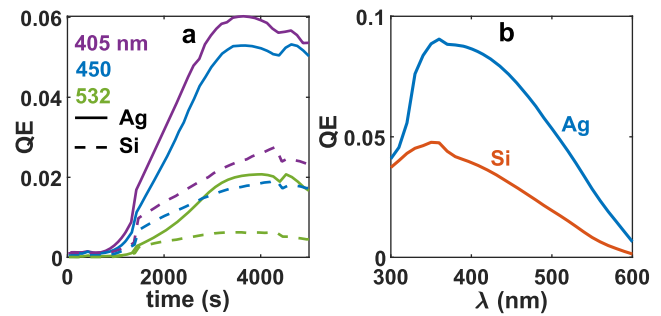


**FIG. 4.** (a) QE measured of the as-grown Cs<sub>3</sub>Sb cathode on Ag (solid line) and Si (dashed line) at 405 nm (purple), 450 nm (blue), and 532 nm (green). The growth was stopped near the Ag peak QE, resulting in the spectral response measurement shown in (b).

Si and Ag simultaneously, and the growth was stopped when the QE on the Ag substrate began to decrease, indicating that the cathode is near the peak QE. The monotonic increase in the Si reference substrate suggests that the QE peak is due to optical effects rather than changes in the surface. Figure 4(a) shows the QE during the growth and again demonstrates clear multiwavelength enhancement on the Ag substrate as compared to the Si substrate. This is reinforced by the full spectral response data in Fig. 4(b). The improvement in QE between Figs. 4(a) and 4(b) is due to the cathode cooling and termination of the growth process and is often seen experimentally. Post-growth XRD analysis was identical for both films, showing a single 220 peak.<sup>34</sup>

The QE and x-ray data together suggest that the results shown are due to optical effects rather than any differences in the photocathode films themselves. Any photocathode can benefit from interference enhancement effects simply by using a smooth metallic substrate, monitoring the QE during growth, and stopping growth when the QE peaks. The high enhancement, particularly near threshold, also suggests that this could be a particularly effective technique for high brightness near threshold photocathode design in an XFEL or UED machine. Going beyond “some” QE enhancement to an optimized interference cathode with maximum brightness will require substantially improved optical constants; these are limited for Cs<sub>3</sub>Sb and essentially nonexistent for Cs<sub>2</sub>Te. A full QE analysis, likely incorporating a Monte Carlo model, is also needed. Special care should also be taken with the metal substrate to minimize roughness. While ultrasMOOTH metal substrates can be produced and are readily available, this method is likely incompatible with the common practice of depositing a cathode directly onto a platen or other bulk metal accelerator components.

The QE data that support the findings of this study are available within the article. More in-depth film growth data and x-ray data are available on request from the authors.

This work utilized the National Synchrotron Light Source II, a U.S. Department of Energy (DOE) Office of Science User Facility operated for the DOE Office of Science by Brookhaven National Laboratory under Contract No. DE-SC0012704. This work was supported by the Office of Science, Office of Basic Energy Sciences of the U.S. Department of Energy under Contract No. DE-SC0013190.

## REFERENCES

- <sup>1</sup>G. R. Fleming and M. A. Ratner, "Grand challenges in basic energy sciences," *Phys. Today* **61**(7), 28–33 (2008).
- <sup>2</sup>P. D. Townsend, "Photocathodes—Past performance and future potential," *Contemp. Phys.* **44**(1), 17–34 (2003).
- <sup>3</sup>A. Creusot and D. Veberič, "Simulation of large photomultipliers for experiments in astroparticle physics," *Nucl. Instrum. Methods Phys. Res., Sect. A* **613**(1), 145–151 (2010).
- <sup>4</sup>L. Zhang, J. P. Hoogenboom, B. Cook, and P. Kruit, "Photoemission sources and beam blankers for ultrafast electron microscopy," *Struct. Dyn.* **6**(5), 051501 (2019).
- <sup>5</sup>N. A. Moody *et al.*, "Perspectives on designer photocathodes for x-ray free-electron lasers: Influencing emission properties with heterostructures and nano-engineered electronic states," *Phys. Rev. Appl.* **10**(4), 047002 (2018).
- <sup>6</sup>H. Zhang *et al.*, "Photoemission experiments of a large area scandate dispenser cathode," *Nucl. Instrum. Methods Phys. Res., Sect. A* **621**(1–3), 79–82 (2010).
- <sup>7</sup>G. J. Caporaso and Y.-J. Chen, "Electron induction linacs," in *Induction Accelerators*, Particle Acceleration and Detection (Springer, Berlin, Heidelberg, 2011), pp. 117–163.
- <sup>8</sup>*Single-Photon Imaging*, edited by P. Seitz and A. J. Theuwissen (Springer, Berlin, Heidelberg, 2011), Vol. 160.
- <sup>9</sup>M. Fiorini *et al.*, "Single-photon imaging detector with O(10) ps timing and sub-10  $\mu\text{m}$  position resolutions," *J. Instrum.* **13**(12), C12005 (2018).
- <sup>10</sup>P. Musumeci *et al.*, "Advances in bright electron sources," *Nucl. Instrum. Methods Phys. Res., Sect. A* **907**, 209–220 (2018).
- <sup>11</sup>W. E. Spicer and A. Herrera-Gomez, "Modern theory and applications of photocathodes," *Proc. SPIE* **2022**, 18–35 (1993).
- <sup>12</sup>D. H. Dowell, "Sources of emittance in RF photocathode injectors: Intrinsic emittance, space charge forces due to non-uniformities, RF and solenoid effects," (Cornell University, 2016); physics arXiv: [arXiv:1610.01242](https://arxiv.org/abs/1610.01242).
- <sup>13</sup>S. Karkare *et al.*, "Reduction of intrinsic electron emittance from photocathodes using ordered crystalline surfaces," *Phys. Rev. Lett.* **118**(16), 164802 (2017).
- <sup>14</sup>M. Gaowei *et al.*, "Synthesis and x-ray characterization of sputtered bi-alkali antimonide photocathodes," *APL Mater.* **5**(11), 116104 (2017).
- <sup>15</sup>A. Alexander, N. A. Moody, and P. R. Bandaru, "Enhanced quantum efficiency of photoelectron emission, through surface textured metal electrodes," *J. Vac. Sci. Technol. A* **34**(2), 021401 (2016).
- <sup>16</sup>W. Liu *et al.*, "Record-level quantum efficiency from a high polarization strained GaAs/GaAsP superlattice photocathode with distributed Bragg reflector," *Appl. Phys. Lett.* **109**(25), 252104 (2016).
- <sup>17</sup>R. K. Li *et al.*, "Surface-plasmon resonance-enhanced multiphoton emission of high-brightness electron beams from a nanostructured copper cathode," *Phys. Rev. Lett.* **110**(7), 074801 (2013).
- <sup>18</sup>S. Karkare and I. V. Bazarov, "Effects of surface nonuniformities on the mean transverse energy from photocathodes," *Phys. Rev. Appl.* **4**(2), 024015 (2015).
- <sup>19</sup>L. Cultrera, C. Gulliford, A. Bartnik, H. Lee, and I. Bazarov, "Ultra low emittance electron beams from multi-alkali antimonide photocathode operated with infrared light," *Appl. Phys. Lett.* **108**(13), 134105 (2016).
- <sup>20</sup>A. Alexander, N. A. Moody, and P. R. Bandaru, "Enhanced photocathode performance through optimization of film thickness and substrate," *J. Vac. Sci. Technol. B* **35**(10), 022202 (2017).
- <sup>21</sup>W. Chang, *Principles of Optics for Engineers* (Cambridge University Press, Cambridge, MA, 2015).
- <sup>22</sup>N. Pinel, C. Bourlier, and J. Saillard, "Degree of roughness of rough layers: extensions of the Rayleigh roughness criterion and some applications," *Prog. Electromagn. Res. B* **19**, 41–63 (2010).
- <sup>23</sup>J. Feng, S. Karkare, J. Nasiatka, S. Schubert, J. Smedley, and H. Padmore, "Near atomically smooth alkali antimonide photocathode thin films," *J. Appl. Phys.* **121**(4), 044904 (2017).
- <sup>24</sup>S. Schubert *et al.*, "Bi-alkali antimonide photocathodes for high brightness accelerators," *APL Mater.* **1**(3), 032119 (2013).
- <sup>25</sup>K. Deutscher and K. Hirschberg, "Thickness dependence of the quantum yield of cesium-antimony films," *Phys. Status Solidi* **27**(1), 145–150 (1968).
- <sup>26</sup>J. R. Sizerlove and J. A. Love, "Analysis of a multiple reflective translucent photocathode," *Appl. Opt.* **6**(3), 443–446 (1967).
- <sup>27</sup>M. A. Novice and J. Vine, "Optical means for enhancing the sensitivity of a tri-alkali photocathode," *Appl. Opt.* **6**(7), 1171–1178 (1967).
- <sup>28</sup>K. L. Jensen, B. L. Jensen, E. J. Montgomery, D. W. Feldman, P. G. O'Shea, and N. A. Moody, "Theory of photoemission from cesium antimonide using an alpha-semiconductor model," *J. Appl. Phys.* **104**(4), 044907 (2008).
- <sup>29</sup>P. B. Johnson and R. W. Christy, "Optical constants of the noble metals," *Phys. Rev. B* **6**(12), 4370–4379 (1972).
- <sup>30</sup>G. Vuye, S. Fisson, V. Nguyen Van, Y. Wang, J. Rivory, and F. Abelès, "Temperature dependence of the dielectric function of silicon using in situ spectroscopic ellipsometry," *Thin Solid Films* **233**(1–2), 166–170 (1993).
- <sup>31</sup>See <https://www.mtixtl.com/Mc-Ag-a-050505S1.aspx> for Ag (Silver) Single Crystal Substrate: {100}, 5 × 5 × 0.5 mm, 1 side polished—McAga050505S1; accessed 23 May 2021.
- <sup>32</sup>M. Gaowei *et al.*, "Codeposition of ultrasmooth and high quantum efficiency cesium telluride photocathodes," *Phys. Rev. Accel. Beams* **22**(7), 073401 (2019).
- <sup>33</sup>Z. Ding *et al.*, "In-situ synchrotron x-ray characterization of K<sub>2</sub>CsSb photocathode grown by ternary co-evaporation," *J. Appl. Phys.* **121**(5), 055305 (2017).
- <sup>34</sup>A. Jain *et al.*, "Commentary: The materials project: A materials genome approach to accelerating materials innovation," *APL Mater.* **1**(1), 011002 (2013).